FT/P7-19

Research and Development of Steady-State EC/ICRF Heating in LHD and an Optimal Remote Steering Antenna

K. Ohkubo, S. Kubo, R. Kumazawa, W. Kasparek1), T. Shimozuma, Y. Yoshimura,
S. Inagaki, Y. Nakamura, K. Saito, T. Seki, T. Mutoh, T. Watari and LHD experimental group

National Institute for Fusion Science, Toki, Gifu, 509-5292, Japan
1) Institut für Plasmaforschung, Stuttgart, Germany
e-mail contact of main author: Ohkubo@nifs.ac.jp

Abstract. In the LHD, steady-state plasma heating by EC wave with 72 kW and ICRF with 0.5 MW was achieved during 756 and 150 sec, respectively. An EC heated plasma with time-averaged radiation temperature of 240 eV and density of less than 1×10^{18} m^{-3} was obtained. As for an ICRF heated plasma, plasmas with electron and ion temperatures of 2 keV and density of 6×10^{18} m^{-3} were sustained until the discharge was terminated by increase in radiation loss. It is confirmed that an imaging property of the remote steering antenna has a branch structure and that recursiveness of input Gaussian beam is found even in a large-angle operation by means of the other branch. The directivity of radiation and power flow are analyzed in detail by using higher-order modes of Hermite-Gauss beam.

1. Introduction

In fusion-oriented experimental devices with superconducting coils such as Tore Supra, TRIAM-1M and LHD, studies on steady-state operation by lower hybrid current drive in tokamaks and ICRF heating in a helical device have been performed intensively. Up to now, two parameters such as discharge duration and input energy were attained to the order of hour and giga-joule in tokamaks. Since establishment of LHD, the steady-state heating by NBI, ICRF and EC waves has been carried out with development of high-power and long-pulse technology. The recent experimental results from steady-state heating on ICRF and EC waves are described. In addition, as to launching technology of millimeter wave by a remote steering antenna, investigations on an extension of the steering angle and optimization of input Gaussian beam were carried out theoretically and compared with experiment. By using the branches on image of both symmetric and asymmetric directions, an injection of Gaussian beam with the extent of 25 degrees enables us for application in ITER with good efficiency.

2. Steady-state EC/ICRF Heating

Steady-state ECH was carried out by an 84 GHz/200 kW diode CW gyrotron with a potential-depressed collector and a chemical vapor deposited diamond window. The high voltage power supplies for the gyrotron had been a little modified to use a body power supply. The body power supply controls the body voltage relative to the collector ground to keep the voltage between cathode and body constant. The gyrotron was installed on one of the gyrotron tanks and connected to the dummy load and transmission line that is extended from the end of evacuated 31.75 mm corrugated waveguide system used for the pre-existing system. Due to the increased reflection from transmission line or the dummy load, the gyrotron test had been limited below 150 kW /1000 sec.

The corrugated waveguide switches were introduced to select power from the pre-existing or the CW gyrotron, to couple the common corrugated waveguide, and to direct power to the dummy load or the LHD antenna. Since the pre-existing mirror antenna system had no cooling channel, the corrugated SUS waveguide of 88.9 mm in inner diameter is used as an

antenna by tapering up the corrugated waveguide from 31.75 mm inside LHD vacuum vessel. Another waveguide switch set just near the LHD port enables to select the mirror or corrugated waveguide antenna to launch an 84 GHz power to the LHD. The transmission line components of 31.75 mm in diameter including a diamond window at the LHD injection port were exchanged or reinforced to increase the heat handling capacities. The temperature rise of the waveguide components on the transmission line was measured by the thermocouples distributed along over the transmission line. In addition, the degree of vacuum on the MOU and the transmission line always was monitored and built in as an inter-lock circuit to avoid an arcing.

In FIG.1, waveforms of parameters are shown. With injecting ECH power of 72kW during 766 sec, an EC heated plasma with time-averaged density of 2.4×10^{17} m^{-3} was sustained without radiation collapse during 756 sec. The density was always controlled by repetitive gas puff not to exceed a density limit for collapse due to limited ECH power. An ECE signal at plasma core increased and that at peripheral region decreased. The time-averaged ECE signal of which optical depth is not sufficiently thick is equivalent of the black body radiation with 240 eV. With time, waveguide temperature raised linearly as shown in FIG. 1.

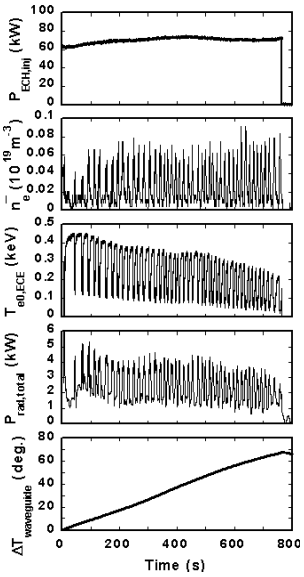

FIG. 1. Waveforms in steady-state ECH

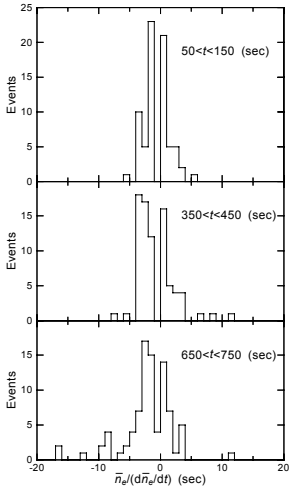

FIG. 2. The appearance counts distribution of the density response time to the gas puffing events for the time intervals of 50 < t <150, 350 <t< 450 and 650 < t< 750 sec in Fig.1.

In the later stage of steady-state heating, decay rate of density just after the gas puffing pulse tends to decrease due to change in recycling from the vacuum wall. Figure 2 shows the appearance counts of the density response time $\bar{n}_e/(d\bar{n}_e/dt)$ to the gas puffing events are plotted for the time intervals of $50<t<150$, $350<t<450$ and $650<t<750$ sec during the discharge shown in FIG. 1. Here, the plus and minus sign of the response time corresponds to the density build-up and decay times after gas puffing, respectively. This figure clearly shows that the density decay time increases towards the end of discharge, while the build-up time stays almost constant. Most of parameters in the gyrotron were kept at the constant or saturated during the pulse. Collector and body voltages were well controlled and kept constant during the shot. Beam and body currents little increased with the time constant of 300 sec and then saturated to be constant toward the end of the pulse. This increase is ascribed to the cathode overheating due to the stray millimeter-wave power near the cathode.

Temperature differences between inlet and outlet of the gyrotron coolant are shown in FIG. 3. Although the coolant temperature near the end of such long-pulse operation increased slightly, it is demonstrated that this gyrotron can be operated well longer than 1000 sec with 200 kW. Pressure rise in the MOU and the waveguides due to the temperature rise had been the major cause of the termination of the pulse. The cooling of the transmission component was enforced during the experimental campaign, but the temperature of some components still kept increasing during 766 sec operation. The outgas from such high temperature component was far from saturation. The pressure inside the waveguide kept increasing due to the poor conductance in the small diameter of the waveguide. As a result, an interlock on degree of vacuum in the MOU and the evacuated waveguide due to the excess outgas was operated and the pulse was terminated. There exists competitive problem on creation of higher-order mode content by slits for increase in pumping speed at the pumping section and on leakage power from the increasing gap for withstanding voltage in the dc-break elements. Outgas in the heated transmission line due to joule loss becomes an important subject for CW power transmission with megawatts level.

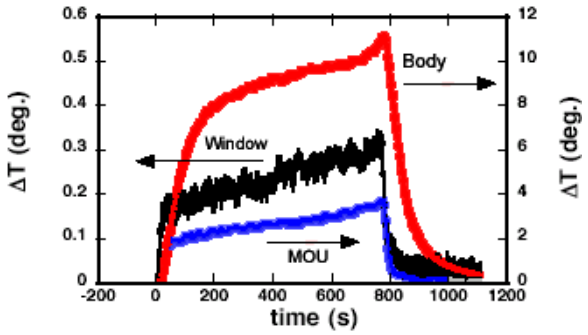

FIG. 3. Time evolutions of temperature differences between inlet and outlet of the coolant at the window, the gyrotron body and the MOU.

Since 1999, the steady-state operation by ICRF heating has been carried out and the pulse length was extended in every experimental campaign, but limited due to a defect on long-pulse operation in an RF generator. Recently, the RF emitter was tuned for the long-pulse operation by installing water-cooled ferrites between control and screen grids to suppress a parasitic oscillation. Time evolutions of plasma parameters of the long-pulse discharge are plotted in FIG. 4; this is the longest plasma discharge so far achieved in the ICRF heated plasma. The plasma with the electron density $\bar{n}_e = 5\sim6\times10^{18}$ m^{-3} and the electron temperature and the ion temperature on the magnetic axis $T_{e0} = T_{i0} = 2.0$ keV was sustained with the ICRF heating power of $P_{RF} = 0.5$ MW. After 90 seconds, the electron density and the radiation power (P_{rad}) increased with time and ended up with $\bar{n}_e = 1\times10^{19}$ m^{-3} and $P_{rad} = 250$ kW before the plasma suddenly disappeared at 150 sec. The operation of the RF generator was automatically suspended by an increasing reflection power due to shrinking the plasma radius, when the plasma was collapsed. An electron density limit of the ICRF heated plasma was examined in the series of the experiments: the critical electron density $\bar{n}_{ecr}$ is given in the relation of $\bar{n}_{ecr}(10^{19}\,\mathrm{m}^{-3}) = 1.8\,P_{RF}(\mathrm{MW})$ [1].

A toroidal asymmetry in Hα intensity observed from the outside ports is shown in the circle-diagram of FIG. 5. Here, the values at $t = 150$ sec are normalized by those at $t = 90$ sec. It is easily found that the increase in Hα is prominent in 3-O and is about 2.5 times larger than that in 8-O. The ICRF heating antennas are installed at 3.5, that is between 3-O and 4-O. This increase in the Hα intensity is believed to be attributed to the temperature increase in the graphite plates located near 3-O in the toroidal direction. A toroidal asymmetry with respect to the temperature increase in the inboard side of the divertor plate is also shown in FIG. 5. It is found that the temperature increase in the 3-I (No.3 of inboard side divertor plate) is prominent. The 3-I divertor plate heated up to 400°C is thought to be a candidate of a hydrogen out-gassing source. This local temperature increase is compared with a calculated

result from particle orbit analysis. Two cyclotron resonance layers are separately located on the mod B surface in the employed magnetic configuration. The behavior of high-energy ions starting at the cyclotron resonance layer was examined using a full orbit calculation code under the RF electric field strength of 20kV/m [2]. About two thousands of high-energy ions with a low initial energy starting from the upper and the lower ion cyclotron resonance layers in various initial phase differences against the RF electric field. As the starting position, 100 points were selected from R = 4.15m to 4.20m along the ion cyclotron layer, where the last magnetic closed surface is at R = 4.14m. Some of them hit the divertor plates within one circulation along the toroidal direction. The toroidal distribution on loss energy of high-energy ions is plotted in FIG. 5 to compare with the measured temperature increase. The orbit calculation suggests that the local temperature increase in divertor plates can be mitigated in two ICRF heating scenarios, in which the ion cyclotron resonance is located on the magnetic axis in the minority heating or is located near the low magnetic field region in the mode conversion heating; there exists no ion cyclotron resonance layer in front of the ICRF heating antennas.

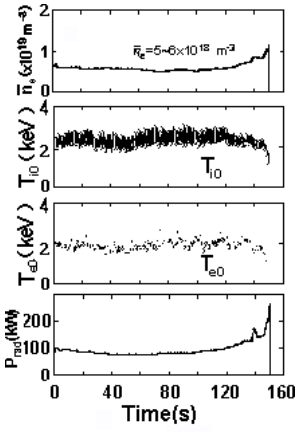

FIG. 4. Waveforms in steady-state ICRF heating.

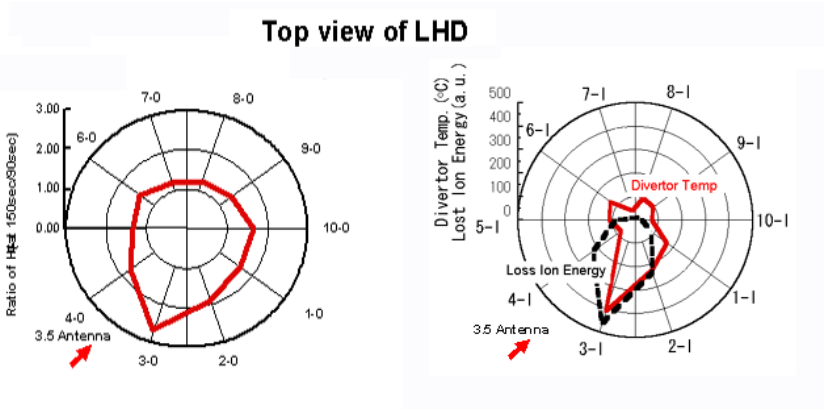

FIG. 5. Distributions along the toroial direction of Hα signal and temperature at the divertor.

3. Branch Structure in a Remote Steering Antenna

To develop an ECH antenna without a steering mirror in the vacuum vessel, characteristics of a square corrugated waveguide antenna with the cross section of $a \times a$ was examined theoretically and experimentally [3, 4]. In addition to the well-known optimum length $L = 4a^2/\lambda$ for small-angle injection, existence of many branches with good imaging for large-angle injection was confirmed [4].

To find out the optimal waist size of injecting Gaussian beam, the imaging characteristics of the remote steering antenna with f = 158 GHz and a = 60.08 mm is calculated for various waist size w_0 as a function of waveguide length L. In FIG. 6, the calculated results for first asymmetric direction with injection angle of 10 degrees and first symmetric one with 15 degrees, respectively are shown. The optimal waveguide length with respect to the imaging efficiency is almost the same for both branches as shown in FIG. 6 (a). Optimal w_0/a on the efficiency of the first asymmetric (symmetric) branch is around 0.30 (0.33). From the viewpoint of range in the waveguide length with the efficiency larger than 90% Δ_{90}, optimal w_0/a is 0.30 for both branches. It is resulted from the minimum number of coupled wavguide modes and the large coupled content in a main mode.

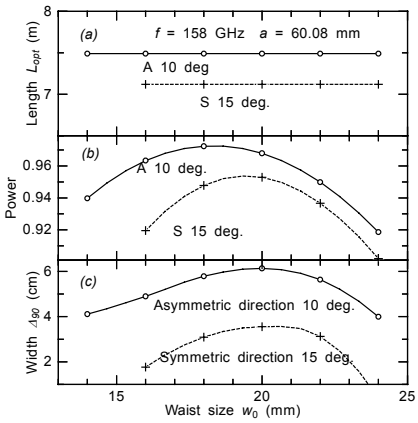

FIG. 6. (a) Optimal waveguide length and (b) imaging efficiency as a function of waist size. (c) The range of waveguide length where the efficiency is larger than 90%. Injection angle on asymmetric and symmetric directions is 10 and 15 degrees.

By changing the frequency instead of the waveguide length, the experimental confirmation of branch structure in recursiveness of input Gaussian beam was performed and compared with the numerical result [4]. All the scanning directions in the calculation and the experiment are perpendicular to the electric field. Calculated (left) and measured (right) results from the radiating power are shown in FIG. 7. Contour plots of (a) upper and (b) lower figures correspond to radiating for asymmetric and symmetric directions. All the data are also normalized with values at the normal injection to the waveguide mouth. Here, L = 6.5 m, a = 60.08 mm and w_0 = 22 mm.

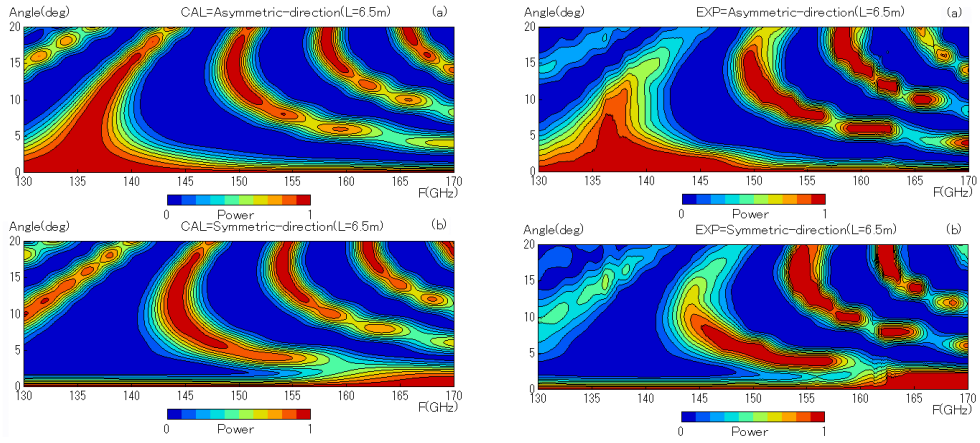

FIG. 7. Calculation (left) and experiment (right). The contour plots of power in (a) asymmetric and (b) symmetric directions with respect to the incident Gaussian beam

The wide contours corresponding to optimum frequency $cL/(4a^2)$ =135.0 GHz at the small-angle injection in the asymmetric direction are seen. As for the second and third branches extending to the larger angle, the optimum frequency in the asymmetric direction is 150 and 158 GHz, respectively. Each branch with the symmetric direction fills partly a corresponding gap in the asymmetric direction. The measured dependence of efficiency (power) on the frequency and injection angle of Gaussian beam is in good agreement with the calculated results [5].

Using the orthonormality on Hermite's polynomial H_m or H_n, the EM fields propagating along the *z'*-axis can be written as the weighted sum of Hermite-Gauss beam HG_{mn} with mode numbers (m, n) and waist size of *w'*. Here, HG_{mn} mode is given by

$$E_{y'} = \frac{1}{w'}\sqrt{\frac{2Z_0}{\pi 2^{m+n} m!n!}} H_m\left(\frac{\sqrt{2}x'}{w'}\right) H_n\left(\frac{\sqrt{2}y'}{w'}\right) \exp\left[-r'^2\left(\frac{1}{w'^2}+\frac{jk_0}{2R'}\right)\right] \exp\left[-jk_0 z' + j(m+n+1)\tan^{-1}\left(\frac{\lambda z'}{\pi w_0'^2}\right)\right]$$

and $H_{x'} = -E_{y'}/Z_0$.

The origins of beam coordinates (x', y', z') and waveguide coordinates (x, y, z) are at the center of the waveguide exit. The weighting coefficient of the HG_{mn} mode, B_{mn} is determined from the output electric field E_y at the waveguide exit using the integration on the waveguide exit: $B_{mn} = -\iint E_y H_{x'}^* dS$

To overview the directivity of radiation, the viewing HG_{m0} beam with the same waist size as an injected fundamental HG_{00} is scanned around y-axis. The x'-z' plane in beam coordinates is on the x-z plane. To analyze a branch where radiation for the symmetric direction is main, waveguide parameters of L = 7.15 m, a = 60.08 mm and f = 158 GHz [4] are used.

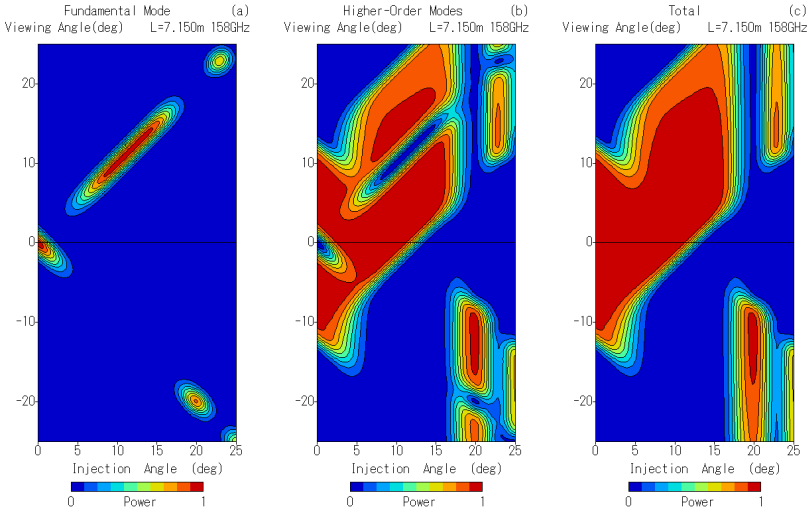

FIG. 8. Contour-plot of power content in the plane of injection and viewing angles. (a) Fundamental mode, (b) higher-order HG modes and (c) total of all the modes. Here, f = 158 GHz and L = 7.150 m. Calculation of the higher-modes is carried out up to m = 60.

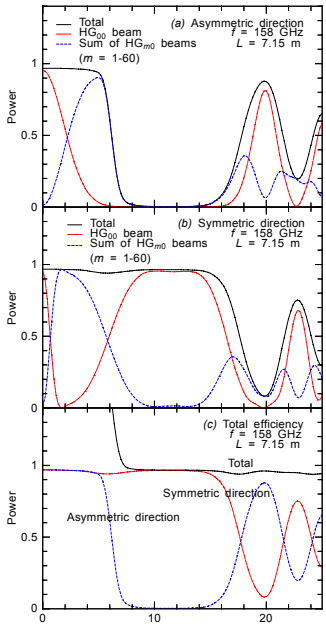

FIG. 9. $|B_{00}|^2$, $\Sigma|B_{m0}|^2$ (except m = 0) and $\Sigma|B_{m0}|^2$ where, L =7.15m.

In FIG. 8, (a) the fundamental mode $|B_{00}|^2$, (b) higher-order modes $\Sigma|B_{m0}|^2$ (except m = 0) and (c) all the calculated modes $\Sigma|B_{m0}|^2$ are contour-plotted in the plane of the injection angle and viewing one. As for higher-order modes, the value B_{m0} is calculated up to m = 60. The width of contour-plot on fundamental mode in FIG. 8 (a) corresponds to around 3θ, where a half angle of beam θ is $\lambda/\pi w_0$. The higher-order HG modes have not central peak profile, which exists in a fundamental mode and its intensity extends to the wing in the profile. This property produces that a fundamental beam propagating along a direction appears as higher-order modes in the viewing beam looking along another direction. As a result, the width of the contour-plot on higher-order modes, which exists on both sides of fundamental mode, increases considerably. On the analysis, the radiating fundamental mode only in symmetric or asymmetric directions is double-counted as higher-order modes looking from the other direction. In the small angle injection, the HG_{00} beam radiates for the asymmetric direction.

With increasing an angle, radiating direction changes to the symmetric one. For the angle larger than 15 degrees, the direction changes again to asymmetric one.

The results from both the asymmetric and symmetric directions and also the total are shown in FIGs. 9 (a), (b) and (c), when a viewing angle is equal to injection one into the waveguide. In the range of 8-16 degrees power is launched for the symmetric direction. In the range larger than 16 degrees, power radiates alternatively for both directions. In the range smaller than 6 degrees, total power content in both directions becomes almost unity by appearance due to double counting as fundamental and higher-order modes in viewing beam as shown in FIG. 9 (c). It is noted that due to truncation of injecting beam, the total is slightly smaller than unity. The boundary angle where double counting disappears is denoted by β_d. When the Gaussian beam with the almost same w_0/a is injected into the smaller-size waveguide, θ increases and β_d increases in proportional to θ. At the intersection points in symmetric and asymmetric contents of FIG. 9 (c), the standing wave is formed near the side-wall of waveguide exit.

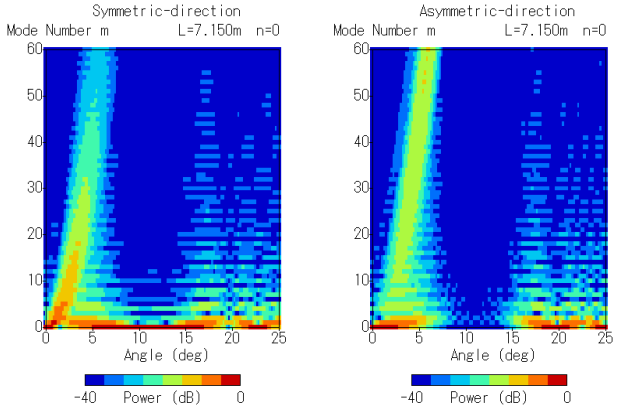

FIG. 10. The mode content of HG_{m0} for symmetric (left) and asymmetric (right) directions as a function of injection angle. Here, the scale of mode content is in decibel unit. Parameters in the figures are the same as those in FIG. 9.

The mode content of HG_{m0} for symmetric and asymmetric directions corresponding to FIG. 9 is shown in FIG. 10, as a function of injection angle. In a small angle lower than 6 degrees, a great number of higher-order modes with very small amount of content compose radiation. In the range of 8-16 degrees, the fundamental mode is main content. In the range larger than 16 degrees, higher-order modes increase to the medium level.

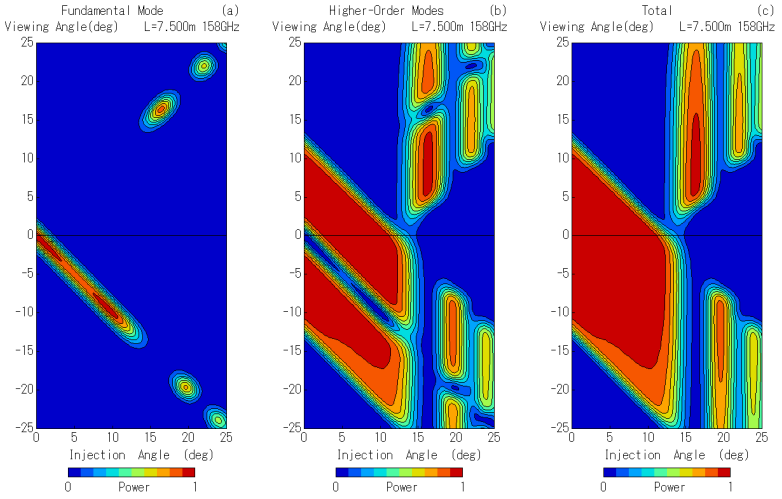

FIG. 11. Contour-plot of power content in the plane of injection and viewing angles. (a) Fundamental mode, (b) higher-order HG modes and (c) total of all the modes. Here, f = 158 GHz and L = 7.50 m. Calculation of the higher-modes is carried out up to m = 60.

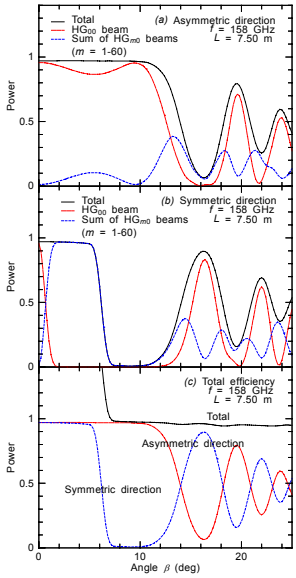

FIG. 12. $|B_{00}|^2$, $\Sigma|B_{m0}|^2$ (except m = 0) and $\Sigma|B_{m0}|^2$ where, L =7.50 m

When the waveguide length increases to L = 7.50 m, the well-known first asymmetric branch appears. As to this branch, the directivity of radiation can be also examined by using the same technique. The contents of fundamental mode and the higher-order modes, and the total are shown as the contour plots on the plane of the injection angle and viewing one in FIGs. 11 (a), (b) and (c), and also plotted for various launching directions in FIGs. 12 (a), (b) and (c) when a viewing angle is equal to injection one for the waveguide. It is understood from the results of FIGs. 11 and 12 that the good imaging of HG_{00} mode is obtained up to injection angle of 12 degrees. By the analysis of mode content such as FIG. 10, it is found that the dip near 5 degrees on the HG_{00} mode is mainly due to a creation of HG_{10} modes. Beyond 15 degrees of injection angle, the main directivity of radiation changes alternatively between asymmetric and symmetric directions.

In FIG. 13, the calculated and the experimental results from the launching for the symmetric direction, where, f = 146 GHz. w_0 = 22 mm, a=60.08 mm and L = 6.5 m. Several curves taking into account of some HG_{m0} modes are drawn. Because frequency of 146 GHz is slightly higher than the optimum value 144 GHz that is shown in calculation in FIG.7, a deep dip in the content of HG_{00} mode appears near 13 degrees. By taking into account of the low-order modes as HG_{10} etc., the experimental results from the detection which are insensitive on the mode-selection can be explained well by the present calculation.

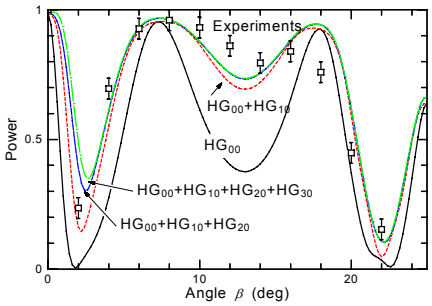

FIG. 13. The launching for the symmetric direction. Here, f = 146 GHz. w_0 = 22 mm, a = 60.08 mm and L = 6.5 m.

4. Summary

We got the expected results in the first steady ECH in LHD despite of mild injection of 72 kW and also obtained medium parameters of density and temperature for steady ICRF heating of 0.5 MW. However, it turns out that wall conditioning and powerful injection are required for increasing density of ECH plasma and that careful treatment of high-energy particles is brought question in order to prolong ICRF heating pulse. The existence of branch structure in the remote steering antenna was found numerically and confirmed experimentally. By using the symmetric branch, we succeeded in the extension of operating angle in the remote steering antenna. The application to the ITER is expected with further development.

References

[1] KUMAZAWA, R. et al., "Density increase during steady-state plasma discharge on the Large Helical Device", P5-108 in 31st European Society Conf. on Plasma Physics (London, 2004).

[2] SAITO, K. et al., "Effects of RF field near ICRF antenna on edge plasma in LHD", to be published in *J. Nucl. Mater.*

[3] OHKUBO, K., "Hybrid modes in a square corrugated waveguide", Int. J. Infrared and Millimeter Waves **22** (2001) 1709.

[4] OHKUBO, K. et al., "Extension of steering angle in a square corrugated waveguide antenna", Fusion Engineering and Design **65** (2003) 657.

[5] OHKUBO, K. and KASPAREK, W., "Extension of operating range in a remote steering waveguide antenna" Conf. digest. of 28th Int. Conf. on IRMMW (Otsu, 2003) p381.